Highly selective conversion of maleic anhydride to γ-butyrolactone over Ni-supported catalysts prepared by precipitation–deposition method

Matías E. Bertone [a], Camilo I. Meyer [a], Silvina A. Regenhardt [a], Victor Sebastian [b,c], Teresita F. Garetto [a], Alberto J. Marchi [a,*]

[a] Catalysis Science and Engineering Research Group (GICIC), INCAPE, UNL-CONICET, Colectora Ruta Nacional 168 Km 0, Paraje El Pozo. (3000) Santa Fe, Argentina
[b] Department of Chemical Engineering and Environmental Technology and Institute of Nanoscience of Aragon (INA), University of Zaragoza, C/Mariano Esquillor, s/n, I+D+i Building, 50018 Zaragoza, Spain
[c] CIBER de Bioingeniería, Biomateriales y Nanomedicina (CIBER-BBN), Campus Rio Ebro-Edificio I+D, 50018 Zaragoza, Spain

ABSTRACT

The gas-phase hydrogenation of maleic anhydride over Ni catalysts supported on SiO_2 and SiO_2–Al_2O_3, prepared by incipient wetness impregnation (I) and constant-pH precipitation–deposition (PD), was studied. The samples were characterized by N_2 adsorption at $-196\,°C$, X-ray diffraction, temperature-programmed reduction, H_2 chemisorption, X-ray photoelectron spectroscopy, and transmission electron microscopy. The catalytic tests were carried out at atmospheric pressure, between 170 and 220 °C and using a space-time of 12 g h mol^{-1}. From the characterization results, it was determined that the interaction between Ni^{2+} species and the support strongly depends on the preparation method. The trend found for the Ni^{2+}-support interaction was Ni/SiO_2-PD >Ni/SiO_2-Al_2O_3-PD > Ni/SiO_2-I. After reduction in H_2 flow, metal Ni particles were one order of magnitude smaller in catalysts prepared by precipitation–deposition than those prepared by impregnation. All catalysts were active for the hydrogenation of maleic anhydride (MA) into succinic anhydride (SA) and subsequent hydrogenolysis to γ-butyrolactone (GBL) and propionic acid (PA). Regardless of small amounts of CH_4, no other products were detected at the reactor outlet. However, the activity and selectivity to GBL depends on the metal particle size, Ni-support interaction and the presence of Lewis acid sites on SiO_2–Al_2O_3 surface. It was found that the small metallic particles obtained by precipitation–deposition method are more active and selective to GBL than the large particles formed using the impregnation method. The highest GBL yield (83%) was reached at 220 °C with Ni/SiO_2–Al_2O_3–PD, which is attributed to selective hydrogenolysis of SA adsorbed on Lewis acid sites by spillover of hydrogen chemisorbed on neighboring metal nickel nanoparticles.

© 2015 Elsevier B.V. All rights reserved.

1. Introduction

In the chemical industry, γ-butyrolactone (GBL) is a pseudo-commodity of remarkable importance, mainly due to its numerous applications as a chemical intermediate [1]. Indeed, one of its main uses is as a starting material for the manufacture of pyrrolidones (2-pyrrolidone and derivatives), which are widely used industrial chemicals [2]. It is also employed for the manufacture of agrochemicals and as a processing aid for production of pharmaceuticals and biodegradable polymers [3]. Furthermore, GBL has a number of primary uses as, for example, an environmentally friendly solvent, replacing chloride solvents (e.g. trichloroethane), a circuit board cleaner in electronics and high technology industries and an electrolyte solvent or additive for Li-ion battery applications [3–6].

GBL is produced worldwide mainly using the following processes: (i) dehydrogenation of 1,4-butanediol, based on the Reppe process, which involves acetylene–formaldehyde condensation [2,7]; (ii) Mitsubishi–Kasei process, based on maleic anhydride (MA) hydrogenation on Ru complexes [8]; (iii) Davy–McKee process, based on hydrogenation of dimethyl or diethyl maleates [9]; and (iv) direct hydrogenation of MA over Ni or Cu catalysts [10,11]. The latter is considered particularly interesting because it is the most direct route for GBL production and does not require the use

of hazardous materials, e.g. acetylene, or expensive noble metal-based catalysts.

A great diversity of catalytic systems and experimental conditions has been reported in the open literature for the hydrogenation of MA. Studies have been carried out both in liquid [3,12–20] and gas phase [4,21–29], as well as in supercritical CO_2 medium [30,31]. The liquid-phase hydrogenation of MA requires high temperatures and hydrogen pressures to obtain substantial GBL yields, and in most cases the use of solvents is needed. For the gas phase hydrogenation of MA, Cu-based catalysts are the most used, often associated with Zn, Cr, Mn, Al, and others. In order to obtain high GBL yields, Cu loadings as high as 40–60%, high catalyst/reactive ratios and/or high operating pressures are needed [21–24]. Besides, Cr-containing catalysts are undesirable due to its toxicity.

In previous works, we tested Cu, Co, and Ni monometallic catalysts impregnated on SiO_2 [32,33], and showed that Ni/SiO_2 catalysts were the most active, selective and stable for the gas-phase MA hydrogenation and succinic anhydride (SA) hydrogenolysis at atmospheric pressure. The influence of the support nature on the performance of Ni-based catalysts prepared by the impregnation method was also investigated and the highest stability and selectivity to GBL was obtained when SiO_2–Al_2O_3 was used as support [34].

Incipient wetness impregnation is a widely used method for catalyst preparation. However, it is known that this method yields a wide distribution of metal particle sizes, especially for medium to high metal contents [34,35]. Instead, precipitation–deposition (PD) method can be used to lay a highly dispersed metal phase onto a support [36]. In order to produce the deposition of the precursors exclusively on the surface of the support and avoid nucleation in the bulk of the solution, conditions must be set and controlled carefully. The development of significant interactions between metal ions and support surface leads to catalysts with small metal particle size, even when high metal loads are used [37,38]. Indeed, depending on the preparation conditions, the precipitated precursors can further react to form a chemical compound with the support [39]. The precipitation–deposition of the solution of a metal ion on a suspended support is generally achieved by inducing a change in the pH of the suspension, either by hydrolysis of dissolved urea or injection of a basic or acid solution. To our knowledge, Ni-based catalysts prepared by precipitation–deposition method have not been tested in the gas-phase MA hydrogenation yet. In this work, precisely, we study the gas-phase MA hydrogenation over Ni catalysts supported on SiO_2 and SiO_2–Al_2O_3 that were prepared by a precipitation–deposition procedure at constant pH developed in our group. A Ni/SiO_2 catalyst was also prepared by incipient wetness impregnation and used as a reference. The objective is to verify the feasibility of improving the catalytic performance of Ni/SiO_2 and Ni/SiO_2–Al_2O_3 on the MA conversion to GBL in gas phase by using the precipitation–deposition method.

2. Experimental

2.1. Catalyst preparation

Ni-supported catalysts were prepared by incipient-wetness impregnation and precipitation–deposition methods. Two insulating oxides were used as supports: SiO_2 (Si, Sigma–Aldrich Grade 62, $S_g = 254 \, m^2 \, g^{-1}$, $V_p = 0.88 \, cm^3 \, g^{-1}$, $D_p = 13.9 \, nm$) and SiO_2–Al_2O_3 (SiAl, Sigma–Aldrich Grade 135, $S_g = 467 \, m^2 \, g^{-1}$, $V_p = 0.67 \, cm^3 \, g^{-1}$, $D_p = 5.54 \, nm$, Si/Al = 6.7), previously conditioned by calcination in air flow at 500 °C.

The sample named Ni/Si–I was prepared by incipient wetness impregnation over SiO_2. The corresponding $Ni(NO_3)_2$ aqueous solution was prepared with the exact concentration to obtain a the-

oretical metal loading of 10 wt.%. Then, this solution was added drop by drop to the support while stirring to form a sludge. The impregnated support was dried overnight and then calcined in air stream at 500 °C for 4 h.

Ni/Si–PD and Ni/SiAl–PD were prepared by a constant pH precipitation–deposition method. A 0.4 M $Ni(NO_3)_2$ aqueous solution was used as the metal precursor, and a 0.5 M K_2CO_3 aqueous solution was used as the precipitating agent. Both solutions were simultaneously added dropwise to a stirred suspension of the corresponding support in deionized water, while the pH was kept in the range of 7.2 ± 0.2 and the temperature at 65 °C by using a controlled thermostatic water bath. The resulting suspension was then filtrated and the so-obtained solid sample was washed with deionized water, dried at 85 °C overnight and calcined in air stream at 500 °C for 4 h.

2.2. Catalyst characterization

Nickel loading was determined by atomic absorption spectroscopy in a PerkinElmer PinAAcle 900T spectrometer. The specific surface area (S_g), pore volume (V_p) and mean pore diameter (D_p) of the oxide precursors obtained by calcination were measured by N_2 physisorption at −196 °C, using a Quantachrome Autosorb-1 sorptometer. Samples were degassed at 250 °C before carrying out the analysis. S_g was estimated by employing the BET equation, while V_p and D_p were determined by the BJH method.

The reducibility of oxide precursors was determined by temperature programmed reduction (TPR) using a Micromeritics AutoChem 2920 unit equipped with a TCD detector. TPR profiles were obtained under a 5% H_2/Ar gas stream (60 $cm^3 \, min^{-1}$) while the temperature was increased from room temperature to 800–900 °C at a rate of 10 °C min^{-1}.

Both oxide precursors and reduced samples were analyzed by X-ray diffraction (XRD), X-ray Photoelectron Spectroscopy (XPS) and Transmission Electron Microscopy (TEM). Taking into account the high phyrophoricity of metal Ni nanoparticles, prior to XRD, XPS and TEM analysis, an ex-situ reduction-passivation procedure of oxide samples was performed as follows: a certain amount of oxide precursor was loaded in a quartz reactor and then reduced at 500 °C or 550 °C, i.e., at the same conditions used to activate them prior to catalytic activity tests. Then, the sample was cooled down to room temperature in flowing N_2, and finally exposed to a 2% O_2/N_2 mixture for 15–20 min [37].

X-ray diffraction (XRD) data of calcined and reduced–passivated samples were recorded at room temperature in a Shimadzu D-1 diffractometer using Cu-Kα radiation (λ = 1.5418 Å) and Ni filter. Analyses were carried out using a continuous scan mode at 2° min^{-1} over a 2θ range of 10–80°. Mean crystallite size was calculated applying Scherrer's equation and considering the diffraction peaks from NiO (0 1 2) planes, for calcined Ni/Si–I, and Ni (1 1 1) planes, for reduced samples.

XPS analyses were performed in a SPECS multianalysis device equipped with a dual Mg/Al X-ray source and a PHOIBOS 150 hemispherical analyzer. Spectra were obtained using the monochromatic Mg Kα radiation with a 200 W source power and a fixed analyzer pass energy of 30 eV, under ultra-high vacuum conditions. Prior to analysis, reduced–passivated samples were subjected to an in situ treatment under a 5% H_2/N_2 flow at 400 °C in order to reduce the surface NiO layer formed during passivation procedure, followed by UHV evacuation for 2 h. Spectral data were processed using CasaXPS software.

Transmission electron microscopy (TEM) observations were carried out using a 200 kV G2 20 S-Twin Tecnai microscope with a LaB6 electron source. Energy dispersive X-ray spectroscopy (EDS) analysis and high angle annular dark field scanning transmission electron microscopy (HAADF-STEM) were performed on

Table 1
Ni content and textural properties of the calcined samples, reduction degree, and irreversible hydrogen chemisorption of the reduced Ni samples.

Sample	Ni load[a] (wt.%)	S_g[b] ($m^2 g^{-1}$)	V_g[b] ($cm^3 g^{-1}$)	D_p[b] (nm)	RT[c] (°C)	RD[d] (%)	V_{H_2}[e] ($Ncm^3 g_{Ni}^{-1}$)
Ni/Si-I	9.5	252	0.85	14.2	500	98	2.6
Ni/Si-PD	9.6	258	0.95	14.7	550	65	16.7
Ni/SiAl-PD	9.4	404	0.55	5.4	500	76	4.0

[a] Metal loading determined by atomic absorption spectroscopy.
[b] Specific surface area (S_g), pore volume (V_g), and pore diameter (D_p) determined from N_2 adsorption data at -196 °C
[c] Reduction temperature during activation in H_2.
[d] Reduction degree calculated after reduction in H_2 flow at RT for 1 h.
[e] Hydrogen irreversibly chemisorbed after activation in H_2 flow at RT for 1 h.

a Tecnai G2-F30 Field Emission Gun microscope operated at 300 kV. To prepare the grid for electron microscopy observations, a reduced–passivated powder sample was dispersed in milli-Q water. After 30 s in an ultrasonic bath, a drop of this suspension was applied to the copper grid (200 mesh) coated with carbon film, and allowed to dry in air.

The hydrogen chemisorption capability of metal Ni was determined by volumetric adsorption at room temperature using a conventional vacuum unit equipped with a MKS Baratron pressure gauge. Oxide precursors were reduced in-situ at 500 °C or 550 °C, i.e. at the same conditions used to activate them prior to hydrogenation reactions. Afterwards, reduced samples were outgassed at reduction temperature for 2 h before chemisorption experiments. Hydrogen uptake was determined using double isotherm method in the pressure range of 0–100 torr.

2.3. Catalytic tests

MA hydrogenation experiments in gas phase were performed at atmospheric pressure in a fixed-bed tubular reactor (SS 1.5 cm i.d.) operated in down-flow mode. Samples were pressed to obtain tablets that were then crushed and screened. The fraction in the range of 0.35–0.42 mm was loaded into the reactor after dilution with quartz using a quartz/catalyst ratio of 1. Catalyst loading (W) of 0.050 g, contact time (W/F^0_{MA}) of 12 g h mol^{-1} and total gas flow rate of 150 $cm^3 min^{-1}$ were used for catalytic tests. Before catalytic tests, the oxide precursor was reduced in-situ under H_2 flow (100 $cm^3 min^{-1}$) for 1 h at 500 °C (Ni/Si–I, Ni/SiAl–PD) or 550 °C (Ni/Si–PD). Then, the reactor was cooled down to the reaction temperature, i.e. between 170 and 220 °C, under flowing H_2. Afterwards, the H_2 stream was switched to a saturator containing molten MA at 75 °C, in order to obtain a H_2/MA gaseous mixture that was continuously fed into the reactor during the 3 h reaction test. Gas stream at the reactor outlet was analyzed by on-line gas chromatography with a Varian CP 3380 unit equipped with a Graphpac GC 0.1% AT-1000 (80–100) packed column and a FID detector. Samples were withdrawn every 15 min, starting at 5 min from the beginning of the catalytic test. Diffusional limitations were ruled out by performing experiments varying particle size and contact time between 0.15–0.60 mm and 10–80 g h mol^{-1}, respectively.

After the catalytic test, the used catalysts were analyzed by temperature-programmed oxidation (TPO). The experiments were performed from 25 to 800 °C, with a heating rate of 10 °C min^{-1}, under an O_2(2%)/N_2 flow of 60 $cm^3 min^{-1}$. The CO_2 in the gas flow exiting the TPO reactor was converted to methane in a second reactor loaded with a Ni/Kieselguhr catalyst operating at 400 °C in H_2 flow [40]. The CH_4 content in the gas stream exiting the methanator was monitored by FID.

3. Results and discussion

3.1. Physicochemical characterization

Ni content and textural properties of Ni/Si–I, Ni/Si–PD and Ni/SiAl–PD samples are shown in Table 1. It was determined that
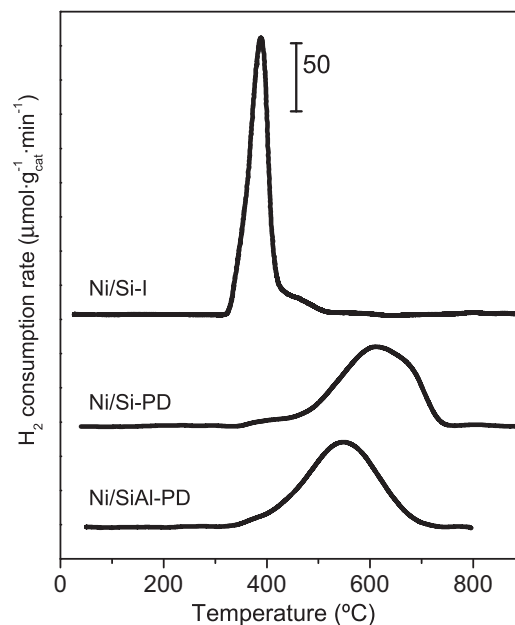
Fig. 1. Temperature-programmed reduction profiles of the calcined samples.

the nickel load was between 9 and 10% in the three samples. Textural properties of SiO_2-supported samples, S_g, V_p and D_p, were similar to those of the corresponding support. This means that neither incipient wetness impregnation nor precipitation–deposition significantly modified SiO_2 textural properties. Instead, a diminution in S_g and V_p of Ni/SiAl–PD sample respect to SiO_2–Al_2O_3 support was observed, while D_p did not change. This can be explained on the basis of some unselective pore blockage during precipitation–deposition process. However, the diminution in specific surface area and pore volume was only about 15% respect to the non-impregnated SiO_2–Al_2O_3.

The TPR profiles of the calcined samples are shown in Fig. 1. In the case of Ni/Si–I, only a single peak between 300 and 450 °C, with the maximum H_2 consumption rate at 390 °C, was observed. This peak is normally assigned to the reduction of large particles of NiO having low interaction with the support [41]. Instead, a very broad peak between 400 and 700 °C was observed for both Ni/Si–PD and Ni/SiAl–PD samples. This H_2 consumption peak can be assigned to the reduction of Ni^{2+} compounds strongly interacting with the support [34]. The absence of a reduction peak at $T < 400$ °C in the case of the PD samples precludes the presence of Ni^{2+} species derived from the precipitation in the bulk of the solution during the preparation stage [39]. In addition, it is worth to notice that the maximum for Ni/Si–PD was 615 °C while for Ni/SiAl–PD it was 550 °C, indicating that Ni^{2+}-support interaction is some stronger when Ni is deposited by precipitation on SiO_2. From these results, the Ni^{2+}-support interaction seems to follow the pattern: Ni/Si–I $\ll$ Ni/SiAl–PD < Ni/Si–PD.

On the base of these TPR evolutions, the activation temperature for each sample (RT, Table 1) was chosen with the aim to
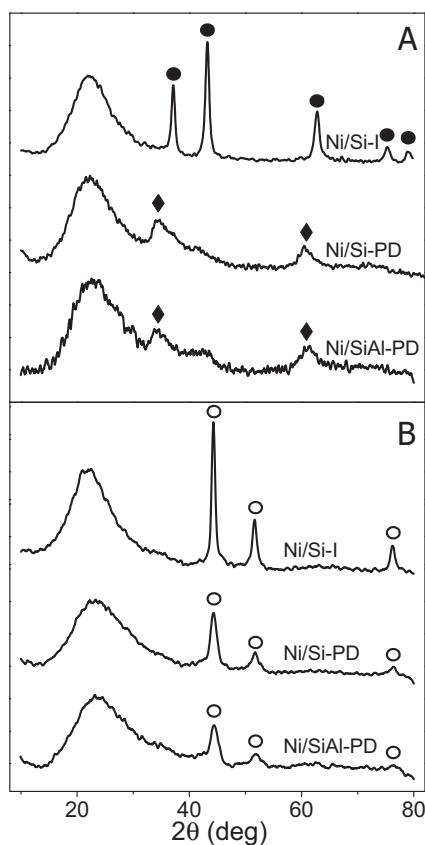
Fig. 2. X-ray diffractograms of the calcined (A) and reduced–passivated (B) samples. (●)NiO (PDF-2-44-1159), (♦) $Ni_3Si_2O_5(OH)_4$ (PDF-2-22-0754), (o) Ni^0 (PDF-2-04-0850).

obtain a significant reduction rate of the Ni^{2+} phase, and avoid support sintering. In order to determine the amount of Ni^{2+} that is actually reduced during activation, the following procedure was followed. First of all, the amount of hydrogen consumed during the TPR experiments (A_C) was calculated from the numerical integration of the corresponding profiles. Then, a new TPR experiment was carried out after in-situ reduction in flowing H_2 at the corresponding RT for each sample. This new hydrogen consumption (A_R) corresponds to the amount of Ni^{2+} that was not reduced in the activation conditions. The reduction degree was then calculated as RD (%) = $(A_C - A_R)/A_C \times 100$, and the results are reported in Table 1. It was found that almost total Ni reduction was obtained for Ni/Si–I sample, but the RD was only 65 and 76% in the case of Ni/Si–PD and Ni/SiAl–PD, respectively. Therefore, the reducibility pattern found is: Ni/Si–I > Ni/SiAl–PD > Ni/Si–PD, which is in agreement with the degree of Ni^{2+}-support interaction stated above from the TPR profiles.

X-ray diffractograms of calcined samples are presented in Fig. 2A. For Ni/Si–I sample, only a NiO polycrystalline phase was observed (PDF-2-44-1159). Estimation of mean crystallite size, calculated considering the diffraction peak from NiO (0 1 2) planes and applying Scherrer's equation, yields a value of 11.5 nm (Table 2). For both PD samples, the diffractograms display broadened peaks that are shifted with respect to those observed for the sample prepared by impregnation. These peaks can be assigned to a Ni hydrosilicate with a pecoraite structure ($Ni_3Si_2O_5(OH)_4$, PDF-2-22-0754). This compound, also called 1:1 Ni phyllosilicate, can be formed by reaction between Ni and support surface, and has already been reported for Ni samples prepared by precipitation–deposition over SiO_2 and SiO_2–Al_2O_3 [38,39]. These X-ray diffractograms are rather similar to the ones obtained for the corresponding samples after

precipitation–deposition and before calcination (not shown here). In consequence, it can be assumed that a cuasi-amorphous and/or highly dispersed phase of nickel hydrosilicates, with crystallite size below 4 nm, was formed during precipitation–deposition process, which are very stable and they are preserved during calcinations. These results are also in agreement with the high Ni^{2+}-support interaction suggested above from TPR results.

Fig. 2B shows the XRD patterns of the reduced-passivated samples. In this case, it was possible to identify a metallic Ni phase (PDF-2-04-0850) for all samples, but with differences in peak intensities and widths. Relative crystalline degree (CD, Table 2), determined from numerical integration of X-ray diffractograms and referred to Ni/Si–I sample, gave the following pattern: Ni/Si–I > Ni/Si–PD > Ni/SiAl–PD. Mean Ni^0 crystallite sizes for each sample, estimated by applying Scherrer's equation to the diffraction peak from Ni (1 1 1) planes, are reported in Table 2 (L_{Ni}^0) and the following trend can be observed: Ni/Si–I > Ni/SiAl–PD ≅ Ni/Si–PD. These results are indicating that metal Ni phase would be more dispersed on samples prepared by precipitation–deposition than on sample obtained by incipient wetness impregnation method.

The volume of irreversibly chemisorbed hydrogen (V_{H_2}) on each reduced sample, expressed per gram of metallic Ni, is shown in Table 1. The lowest amount of chemisorbed hydrogen was observed with Ni/Si–I and the pattern found in this case was: Ni/Si–PD > Ni/SiAl–PD > Ni/Si–I. From this pattern, it is clear that both preparation method and support have a very strong influence on the hydrogen chemisorption capability of metal nickel phase. On the other hand, according to these results and assuming a stoichiometry H/Ni = 1 [33], the amount of surface metal Ni should follow the same order as that shown above for the volume of hydrogen chemisorbed irreversibly. However, this is not in agreement with the results obtained by XRD, which show crystallites of similar mean sizes in Ni/SiAl–PD and Ni/Si–PD (Fig. 2 and Table 2), suggesting similar surface Ni^0 concentrations for both samples. Taking into account the discrepancies between both characterization techniques in relation to the amount of exposed metal Ni, additional evidence was gathered by XPS and TEM. The results obtained are described and discussed as follows.

XPS results corresponding to the Ni 2p region, both for calcined (A) and for reduced (B) samples, are presented in Fig. 3. The binding energy scale was adjusted by shifting the C 1s peak position to 284.6 eV. Background was subtracted according to the Shirley method and peaks were fitted using a combination of Gaussian and Lorentzian peak functions.

For calcined Ni/Si–I (Fig. 3A), a very low signal corresponding to Ni $2p_{3/2}$ at 855(0.2) eV was assigned to NiO [37]. For samples prepared by PD, the signal corresponding to Ni $2p_{3/2}$ was shifted to 856.4 eV. This shift was attributed to the formation of Ni–Si compounds such as $NiSiO_3$, Ni_2SiO_4 or hydrosilicates [37,42,43]. This assignment was made by taking into account not only peak positions, but also the 1.4 eV difference in binding energy between NiO and nickel silicate species, and the 6.2 eV shift of the satellite peaks to higher binding energies, which rules out the presence of Ni^{3+}. The presence of these Ni–Si compounds in calcined samples prepared by PD method is in good agreement with the strong Ni^{2+}-support interaction evidenced from TPR and XRD results described and discussed above.

In the case of the reduced samples, the spectra in the Ni $2p_{3/2}$ region (Fig. 3B) presents a main signal at 851.8 eV ascribed to Ni^0 [43] and a somewhat important contribution of Ni^{2+} species with BE at 855(0.2) eV and 856.4 eV, similar to the corresponding calcined samples. These results are consistent with the incomplete reduction of samples prepared by PD (RD, Table 1). It is important to notice that, in the case of Ni/Si–I the low signal/noise ratio is indicative of a relatively low specific Ni^0 surface area. The low Ni 2p signal intensity for this sample compared to Ni/Si–PD and

Table 2
Catalyst characterization data from XRD, XPS, and TEM.

Sample	CD[a] (%)	L_{Ni^0}[b] (nm)	SCP_{Ni^0}[c]	S_{Ni^0} (μmol g_{cat}^{-1})	d^{Ni^0}[f] (nm)	$d_{TEM}^{Ni^0}$[g] (nm)
Ni/Si-I	100	11.5	0.038	23.0[d]	71.4	71
Ni/Si-PD	59	5.9	0.33	205.2[e]	5.2	4
Ni/SiAl-PD	46	4.9	0.5	297.1[e]	4.1	4.5

[a] Crystallinity degree relative to reduced Ni/Si–I sample from X-ray diffractograms.

[b] Ni^0 mean crystallite size calculated using Scherrer's equation from Ni(1 1 1) planes.

[c] Ni^0 surface concentration parameter from XPS Ni2p level spectra.

[d] Atomic concentration of surface metallic Ni; determined from H_2 chemisorption, assuming a chemisorption stoichiometry H/Ni = 1.

[e] Atomic concentration of surface metallic Ni relative to Ni/Si–I estimated from SCP_{Ni^0}.

[f] Metallic Ni average particle size, calculated from S_{Ni^0} values, assuming spherical particle shape for Ni/Si–I and hemispherical geometry for Ni/Si–PD and Ni/SiAl–PD.

[g] Metallic Ni average particle size estimated from TEM images by counting 100–130 particles.
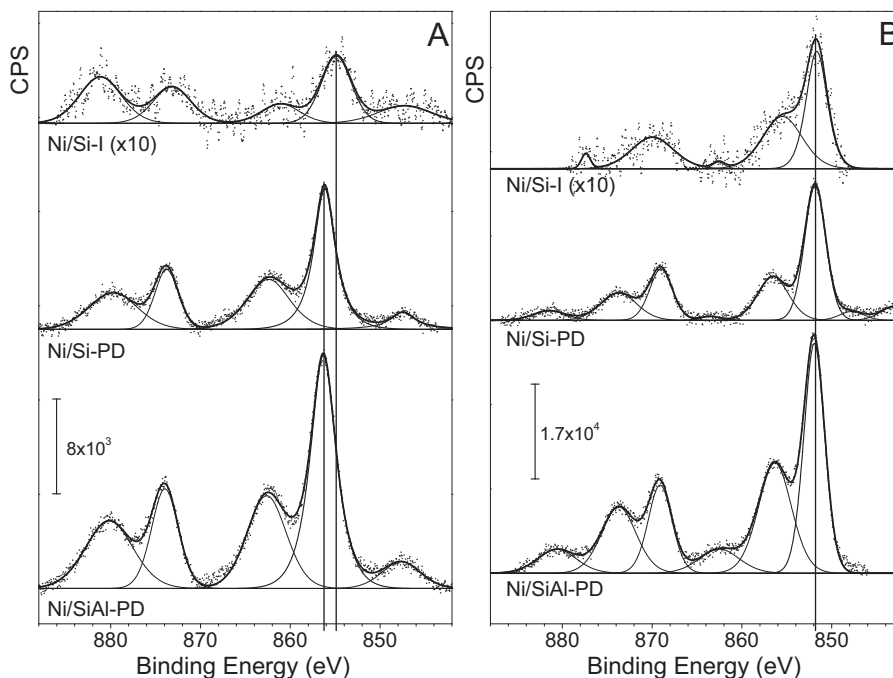
Fig. 3. XPS spectra in the Ni 2p region of the calcined (A) and reduced (B) samples.

especially to Ni/SiAl–PD, does not seem quite consistent with the volumes of H_2 chemisorbed irreversibly. It is well established that the intensities of the XPS peaks for a given element are directly proportional to its surface concentration. Therefore, a relative metallic Ni surface concentration parameter $\left(SCP_{Ni^0}\right)$ could be estimated from Ni $2p_{3/2}$ and Si 2p intensities for each of the reduced samples using the following expression:

$$SCP_{Ni^0} = \frac{\left(A_{Ni^0}/SF_{Ni}\right)/\left(A_{Ni^0}/SF_{Ni} + A_{Ni^{2+}}/SF_{Ni} + A_{Si}/SF_{Si}\right)}{X_{Ni}/(X_{Ni} + X_{Si})}$$

where:

A_{Ni^0}: Metallic Ni peak intensity (Ni $2p_{3/2}$ region)

$A_{Ni^{2+}}$: Ni^{2+} peak intensity (Ni $2p_{3/2}$ region)

A_{Si}: Si^{4+} peak intensity (Si 2p region)

SF_{Ni}: Ni $2p_{3/2}$ experimental sensitivity factor

SF_{Si}: Si 2p experimental sensitivity factor

X_{Ni}: Bulk Ni atomic fraction calculated from elemental composition

X_{Si}: Bulk Si atomic fraction calculated from elemental composition

So defined, SCP_{Ni^0} is proportional to Ni^0 surface concentration. Hydrogen chemisorption has been previously used to estimate surface metal concentration when Ni is impregnated on SiO_2 [33].

Therefore, based on V_{H2} and assuming a H/Ni = 1 chemisorption stoichiometry, the surface metal Ni concentration was calculated for this sample and is presented on Table 2 (S_{Ni^0} column, first line). Hence, from SCP_{Ni^0} (Table 2) and S_{Ni^0} for the impregnated sample, the metallic Ni surface concentration was estimated for both PD samples (S_{Ni^0} column, second and third lines). From these values, it was possible to estimate a mean Ni^0 particle size $\left(d_P^{Ni^0}\right)$ for all of the reduced samples (Table 2). It was concluded that, for similar Ni content, samples prepared by PD have an exposed metallic Ni surface concentration an order of magnitude higher than Ni/Si–I and, as a consequence, a metal Ni particle size about fifteen times lower. These values, in agreement with XRD measurements, indicate that metal Ni phase on the support surface of PD samples has a much higher dispersion than that of the impregnated sample. The reduced–passivated samples were then subjected to observation by TEM in order to verify the certainty of this conclusion.

Representative TEMs for reduced–passivated samples are shown in Fig. 4 A, B, C and E, where metallic Ni particles appear as the dark zones in the micrographs. Furthermore, HAADF-STEM micrographs for PD samples are also shown (Fig. 4D and F), in which contrast is inverted respect to conventional TEM (Z-contrast). EDS analysis (not shown) was performed on these samples, confirming that bright particles are metallic Ni. The filament-like structures
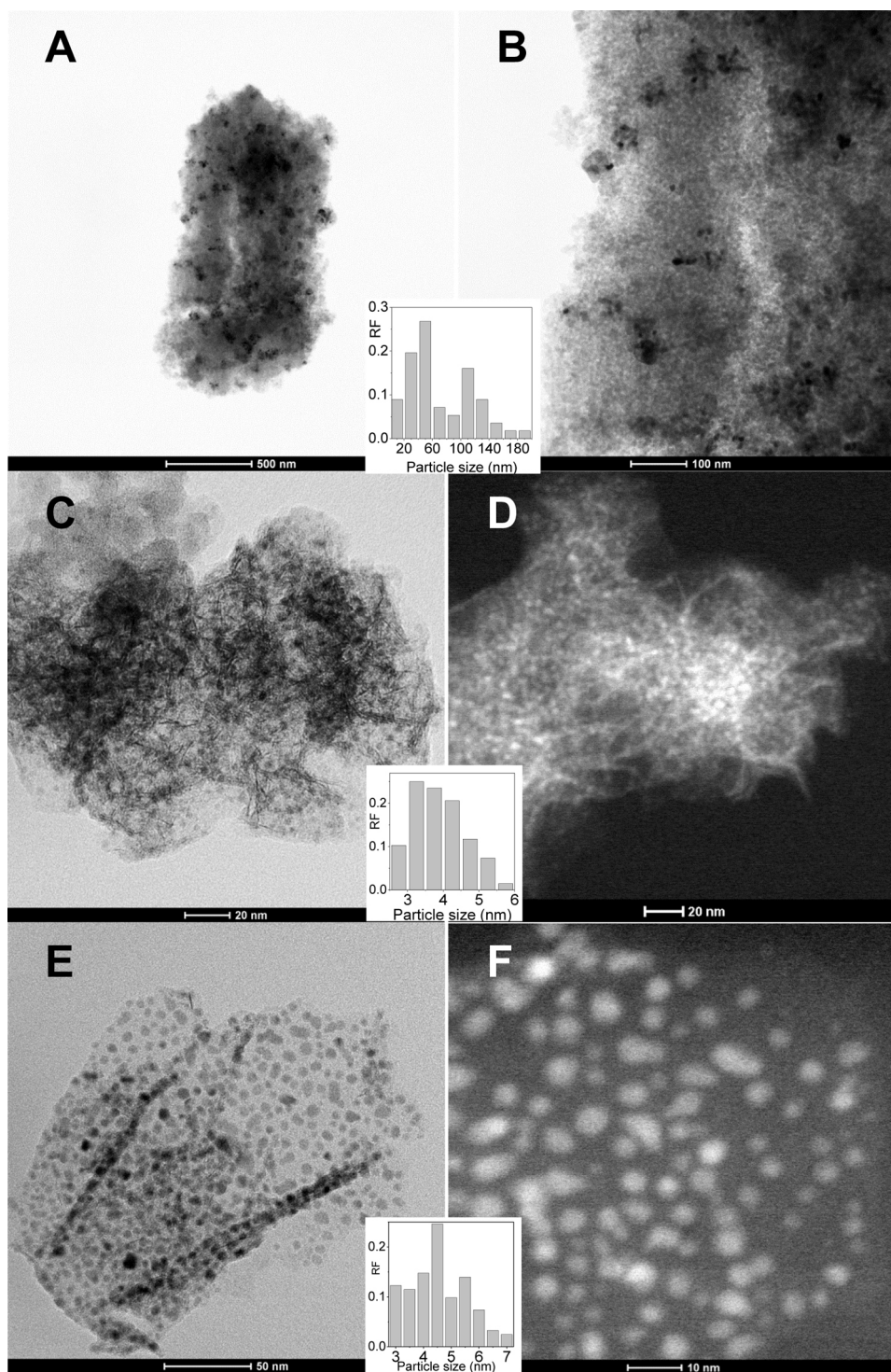
Fig. 4. TEM (A and B) micrographs of reduced Ni/Si–I, TEM (C) and STEM (D) micrographs of reduced Ni/Si–PD, and TEM (E) and STEM (F) micrographs of reduced Ni/SiAl–PD. Histograms of particle size distributions as insets.

observed in Ni/Si–PD (Fig. 4C and D) and, in lesser extent, in Ni/SiAl–PD (Fig. 4E) are usually assigned to a nickel hydrosylicate phase [37], in agreement with the incomplete reduction of Ni^{2+} in PD samples at the corresponding RT.

A metallic Ni particle size distribution was determined for the three samples, by counting 100–130 particles from several micrographs, and the corresponding histograms are shown as insets in Fig. 4. Ni/Si–I showed a wide range of particle sizes, from 14 to 184 nm, with a bimodal distribution and a mean particle

size of 71 nm, in agreement with the value determined from H_2 chemisorption (Table 2, 71.4 nm). Instead, PD samples showed a monomodal and much narrower distribution, with particle sizes in the 3–7 nm range, and a mean size of 4 nm for Ni/Si–PD and 4.5 nm for Ni/SiAl–PD. These values are very close to those calculated for these samples from S_{Ni^0} (Table 2), indicating that H_2 chemisorption is affected by both preparation method and type of support. Therefore, the chemisorbed H_2 volumes determined in this work can not be used to estimate particle size of Ni-based catalysts when

they are prepared by precipitation–deposition. It is worth noticing that Ni/Si–PD is able to chemisorb much more hydrogen than Ni/SiAl–PD even when the former has a lower Ni^0 surface concentration. In consequence, it seems that chemisorption stoichiometry does not only depend on the preparation method but also on the support.

In addition, the metallic Ni mean particle size $\left(d_P^{Ni^0}\right)$ and mean crystallite size $\left(L_{Ni^0}\right)$ are almost the same for both samples prepared by PD, indicating that each particle is mainly comprised of a single crystallite and no agglomeration occurs during activation (Table 2). On the other hand, for Ni/Si–I, the $d_P^{Ni^0}/L_{Ni^0}$ ratio is around 7, indicating that an extensive agglomeration occurs during impregnation and/or calcinations steps. Agglomeration during activation is discarded because TEM micrographs for calcined Ni/Si–I (not shown) display big NiO particles, with a size distribution similar to that of the reduced sample. The fact that Ni^0 crystallites agglomerate in Ni/Si–I but do not agglomerate in the catalysts prepared by PD, is in agreement with the stronger metal-support interaction of the latter, as it was established from TPR, XRD and XPS results.

In summary, it was stated that a much stronger interaction between Ni phase and support can be achieved by using precipitation–deposition method than incipient wetness impregnation. This strong interaction yields, after the reduction process, a metallic Ni phase comprised of very small particles between 3 and 6 nm in size, homogeneously distributed on the support surface. Therefore, PD samples expose a much larger metallic Ni surface area per gram of catalyst than the reduced Ni/Si–I sample, in spite of the incomplete reduction achieved. In spite of the higher metallic Ni dispersion on PD samples, the ratio of irreversible chemisorbed H_2 to surface metal Ni (H/Ni) was lower over Ni/Si–PD and Ni/SiAl–PD samples than over Ni/Si–I. This is indicating that Ni-support interaction is reducing the capability of metal Ni phase for dissociative hydrogen chemisorption.

3.2. Catalytic tests

All the catalysts reported in this work were highly active for MA hydrogenation, reaching conversions of ca. 100% that remained constant throughout the catalytic test. According to previous results [33], the reaction pathway for MA hydrogenation over Ni-based catalysts at atmospheric pressure is as follows: (1) MA is hydrogenated into SA; (2) SA is converted to GBL (+H_2O) and PA (+CO) through parallel hydrogenolysis reactions; (3) GBL is converted into PA (+CH_4) through a subsequent hydrogenolysis reaction. Considering that hydrogenation of MA to SA and hydrogenolysis of SA to GBL and PA are consecutive reactions, the SA conversion was calculated as $X_{SA} = X_{MA} - Y_{SA}$, where X_i (i: SA, MA) is the corresponding conversion and Y_{SA} is the amount of SA that was not converted to GBL and/or PA. From now on, initial conversion, yield and selectivity are assumed to be those corresponding to 5 min reaction time.

SA conversions as a function of time, for the three catalysts, at 170 °C, 195 °C, and 220 °C are shown in Fig. 5A, B, and C, respectively. For Ni/Si–I, SA conversion remained constant during 3 h reaction time, being 13% at 170 °C, 30% at 195 °C and 62% at 220 °C. The conversion of SA as a function of time for Ni/Si–PD showed a decrease at the three temperatures. At 170 °C, X_{SA} dropped from 24 to 18% after 150 min of reaction, and then kept constant. At 195 °C the conversion decreased from 56 to 45% and stabilized at this value after about 120 min. At 220 °C the initial conversion was 89% and stabilized at 80% after 60 min of reaction. Hence, in all cases the diminution in conversion was around 6–9% before reaching the level of residual activity. In a previous work [32], the catalyst deactivation with residual activity has been attributed to

the competitive effect of carbonaceous compound deposition and regeneration by hydrogenation of unsaturated compounds strongly adsorbed on the catalyst surface. The relative rate of both surface reactions defines the global deactivation rate as well as the time to reach the steady state. The initial deposition rate of carbonaceous compounds over Ni/Si–PD increased with temperature, explaining the trend observed for deactivation rate. Accordingly, the time in which regeneration rate equals carbon deposition rate diminished as the temperature was raised. In the case of Ni/SiAl–PD, a slow deactivation was always observed between 170 °C and 220 °C: SA conversion diminished from 31% to 27% at 170 °C, from 70% to 63% at 195 °C and from 100% to 96% at 220 °C during the 3 h catalytic test. These evolutions indicate that the time to equal the carbon deposition and regeneration rates is higher for Ni/SiAl–PD than for Ni/Si–PD, but global deactivation rate is much lower with Ni/SiAl–PD than with Ni/Si–PD.

In summary, both the initial and the steady state conversions of SA with Ni/SiAl–PD were always higher than with Ni/Si–PD and Ni/Si–I. Therefore, the pattern found for the activity in SA hydrogenolysis between 170 °C and 220 °C was: Ni/SiAl–PD > Ni/Si–PD > Ni/Si–I.

The only hydrogenolysis products detected in all cases were GBL, PA and CH_4, in agreement with previous results obtained for the gas-phase MA hydrogenation over Ni-based catalysts [33]. The GBL yield for all catalysts at 170, 195 and 220 °C is presented in Fig. 6A, B, and C, respectively, and in Table 3. The pattern found for the initial and steady-state yield in GBL, between 170 °C and 220 °C, was the same as that observed for the activity in SA hydrogenolysis. The highest initial yield in GBL, 91%, and after 3 h of reaction, 83%, was obtained with Ni/SiAl–PD at 220 °C. The evolutions of GBL yield with time were also similar to those observed for SA conversion (Fig. 5). For Ni/Si–I catalyst the GBL yield remained constant at the three temperatures, with values of 7% at 170 °C, 14% at 195 °C and 33% at 220 °C, i.e., about half of the SA conversions at the same temperatures. Instead, a decay of 5–10% for the yield in GBL was observed with Ni/Si–PD and Ni/SiAl–PD. However, in the steady state, almost 90% of SA was converted to GBL on Ni/SiAl–PD, while around 55–65% of SA was converted to GBL on Ni/Si–PD catalyst.

In all of the cases, the other product from SA hydrogenolysis was PA. The yield in PA was nearly constant or a slight increase was detected with time on stream, i.e., the time evolutions of PA yield are different to those observed for GBL yield (Figs. 6 and 7). The values reached after 3 h are summarized in Table 3 along with GBL yield. In general, PA yield increased as the temperature was raised. The lowest yield in PA at the three temperatures used in this work was always obtained with Ni/SiAl–PD.

The yield in CH_4 was lower than 2% at $T \leq 195$ °C and less than 4% at $T = 220$ °C with the three Ni-based catalysts. Besides, CH_4 yield was always less than one tenth of the yield in GBL, indicating that GBL hydrogenolysis was unimportant respect to SA conversion. These results are in agreement with a previous work [33] where it was already shown that, over Ni supported catalysts and in the experimental conditions used in this work, PA is mainly coming from SA hydrogenolysis, in parallel with GBL. Then, the selectivity to GBL was defined as $S_{GBL} = Y_{GBL}/(Y_{GBL} + Y_{PA})$ and the corresponding values are shown in Table 3. It can be seen that, in the whole temperature range, the trend in selectivity to GBL is the following: Ni/SiAl–PD > Ni/Si–PD ≥ Ni/Si–I. Besides, taking into account the different time evolutions for the GBL and PA yields for each catalyst, and the low yields in CH_4, it can be assumed that parallel hydrogenolysis of SA to GBL (SA → GBL) and SA to PA (SA → PA) take place on different types of hydrogenolytic sites [33,34]. It is then clear that the sites that suffer deactivation in Ni/Si–PD and Ni/SiAl–PD are SA → GBL sites and not SA → PA sites.

The influence of the preparation method on the performance of Ni-based catalysts can be evaluated by comparing Ni/Si–I and
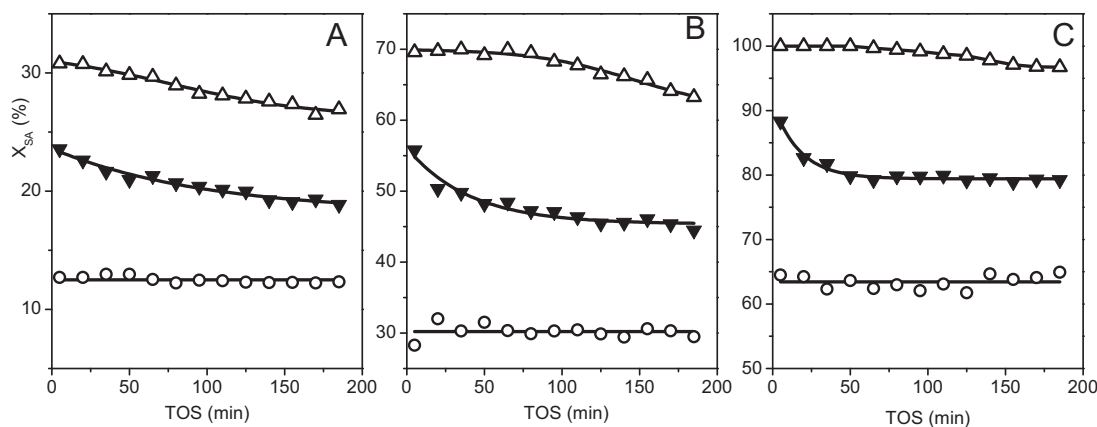
Fig. 5. Succinic anhydride conversion (X_{SA}) as a function of time at (A) 170 °C, (B) 195 °C and (C) 220 °C. (P = 1 bar, W/F^0_{MA} = 12 g h mol^{-1}). (◯) Ni/Si–I, (▼) Ni/Si–PD, (△) Ni/SiAl–PD.
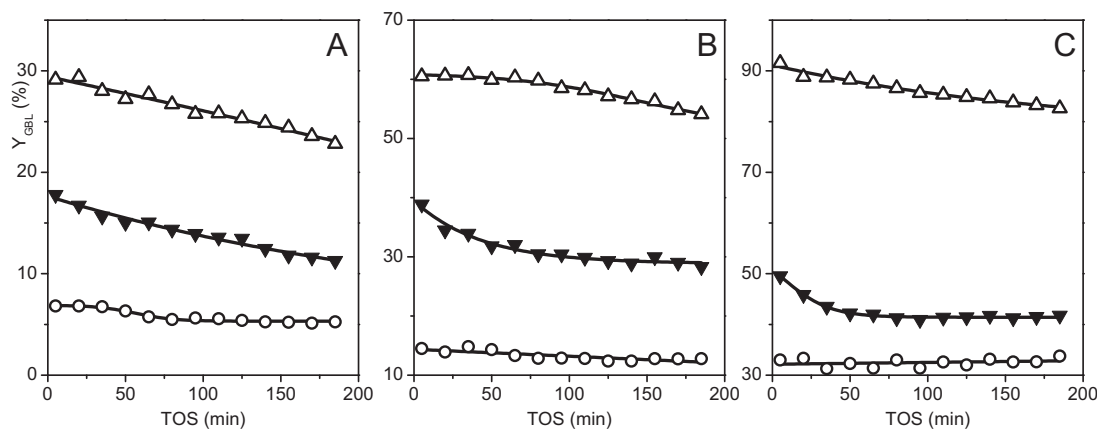
Fig. 6. γ-butyrolactone yield (Y_{GBL}) as a function of time at (A) 170 °C, (B) 195 °C and (C) 220 °C. (P = 1 bar, W/F^0_{MA} = 12 g h mol^{-1}). (◯) Ni/Si–I, (▼) Ni/Si–PD, (△) Ni/SiAl–PD.

Table 3
GBL and PA yield and selectivity to GBL at different reaction temperatures $\left(P_{tot} = 1\,\mathrm{bar},\ W/F^0_{MA} = 12\,\mathrm{ghmol^{-1}}\right)$.

Catalyst	T (°C)	Y_{GBL}[b] (%)	Y_{PA}[a] (%)	S^0_{GBL}[b] (%)	S_{GBL}[a] (%)	r^0 x 10²[b] $\left(\mathrm{mol_{SA}\,h^{-1}\,m^{-2}_{Ni^0}}\right)$
Ni/Si–I	170	5.2	6.4	54.4	44.8	1.22
	195	12.7	15.8	48.7	44.6	2.81
	220	33.0	27.5	54.4	54.5	6.18
Ni/Si–PD	170	10.7	5.4	80.5	68.2	0.25
	195	29.1	15.6	71.2	65.2	0.60
	220	41.5	33.8	59.7	55.2	0.95
Ni/SiAl–PD	170	23.6	2.6	93.5	90.4	0.23
	195	55.1	8.8	87.6	86.2	0.52
	220	83.2	10.7	93.8	88.7	0.74

[a] GBL and PA yield (Y_{GBL}, Y_{PA}) and GBL selectivity (S_{GBL}) after 3 h of reaction.
[b] Initial GBL selectivity $\left(S^0_{GBL}\right)$ and initial specific rate of SA hydrogenolysis (r^0).

Ni/Si–PD. In spite of its deactivation, Ni/Si–PD is more active for SA hydrogenolysis at all temperatures studied (Fig. 5) and shows a higher GBL selectivity at $T \leq 195$ °C (Table 3) than Ni/Si–I. The increase in the overall hydrogenolysis activity is in agreement with the larger exposed metal surface of smaller particles on Ni/Si–PD catalyst (S_{Ni^0}, Table 2). However, the specific initial SA hydrogenolysis rate was much lower for Ni/Si–PD than for Ni/Si–I (Table 3, r^0). This is not surprising, since it is known that most hydrogenolysis reactions are structure-sensitive and, in some cases, small particles have a lower specific activity than large ones. In consequence, even though having a lower intrinsic activity for SA hydrogenolysis, Ni/Si–PD has a higher concentration of hydrogenolytic sites per

gram of catalyst than Ni/Si–I, due to its larger metallic Ni surface area. The observed effect is a higher overall hydrogenolytic activity.

The higher selectivity to GBL at $T \leq 195$ °C of Ni/Si–PD respect to that of Ni/Si–I can be explained considering that the ratio of SA → GBL sites to SA → PA sites is higher on Ni/Si–PD than on Ni/Si–I. In other words, as Ni particle size diminishes, the ratio between surface concentration of SA → GBL hydrogenolytic sites and SA → PA hydrogenolytic sites increases, which leads to an enhancement in GBL selectivity. This increase in selectivity also seems to be related to the capability for the dissociative hydrogen chemisorption of the metal Ni phase of each catalyst. The H/Ni ratio for each catalyst can be estimated by dividing V_{H2} values (Table 1,
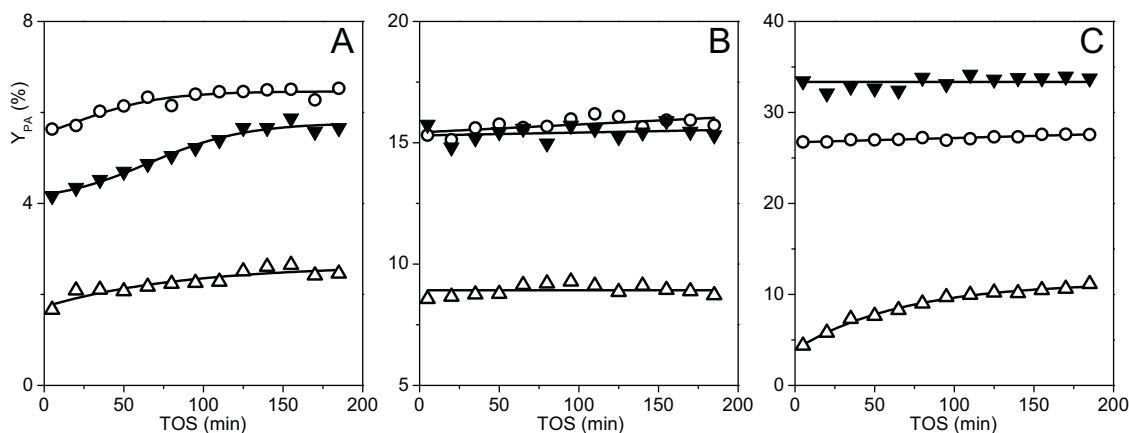
Fig. 7. Propionic acid yield (Y_{PA}) as a function of time (A) 170 °C, (B) 195 °C and (C) 220 °C. ($P = 1$ bar, $W/F^0_{MA} = 12$ g h mol^{-1}). (○) Ni/Si–I, (▼) Ni/Si–PD, (△) Ni/SiAl–PD.

last column) by S_{Ni^0} values (Table 2, fifth column) after making the corresponding unit conversion. Thus, an H/Ni ratio of 0.47 is obtained for Ni/Si–PD relative to Ni/Si–I. In consequence, Ni^0 surface on Ni/Si–PD is less active for the dissociative H$_2$ chemisorption and more selective for SA hydrogenolysis to GBL than the one on Ni/Si–I.

Great differences are still found when both catalysts prepared by PD are compared, which indicates a strong influence of support nature. Ni/SiAl–PD is more active in the selective SA hydrogenolysis into GBL than Ni/Si–PD (Fig. 5 and Table 3). However, the initial specific rate for SA hydrogenolysis is almost the same for both PD catalysts (Table 3). This result is in agreement with the fact that both catalysts have similar Ni^0 average particle size (4–4.5 nm, Fig. 4) and particle size distribution, as discussed in Section 3.1. Then, the higher overall hydrogenolytic activity of Ni/SiAl–PD respect to Ni/Si–PD can be attributed to the higher metallic Ni surface area (S_{Ni^0}, Table 2) of Ni/SiAl–PD.

A significant difference in GBL selectivity was also observed between both PD samples (Table 3). For Ni/Si–PD, the initial selectivity to GBL was between 60% and 80% but diminished to 55–70% after three hours, depending on the temperature. Besides, selectivity to GBL diminished with temperature because SA → PA rate was favored over SA → GBL rate on Ni/Si–PD as temperature was raised from 170 °C to 220 °C. Instead, for Ni/SiAl–PD, selectivity to GBL was always between 87% and 94%, diminishing slightly with time on stream, while keeping almost constant with temperature. In consequence, it is expected that the ratio of SA → GBL sites to SA → PA sites would be much higher when the metal Ni phase is supported on SiO$_2$–Al$_2$O$_3$ than on SiO$_2$. Clearly, this difference in selectivity cannot be attributed to a difference in metallic particle size as when comparing both catalysts prepared over SiO$_2$. The different nature of the supports must then be playing an important role on hydrogenolytic activity that goes beyond Ni^0 particle size. The results from DRX and XPS do not evidence a great difference in Ni^{2+}-support interaction between both calcined samples. Besides, an electronic effect of SiO$_2$–Al$_2$O$_3$ on Ni^0 particles is not evidenced from XPS of the reduced samples. Only some difference was detected by TPR, since Ni^{2+} precursor was more easily reduced when the support was SiO$_2$–Al$_2$O$_3$ instead of SiO$_2$ (Fig. 1). A plausible explanation is that the interaction of Ni^{2+} phase with SiO$_2$–Al$_2$O$_3$ influences the reduction to Ni^0 in a different way that the Ni^{2+}–SiO$_2$ interaction does. As a consequence, the type of metal Ni phases exposed on the surface could be different in both cases. The results obtained by H$_2$ chemisorption are in agreement with this assumption. For Ni/SiAl–PD, the H/Ni ratio, estimated from V_{H2} and S_{Ni^0} as described before, yields a value of H/Ni = 0.1 that is even lower than the one obtained for Ni/Si–PD (H/Ni = 0.47). In

agreement with the stated above, the sample with less capability for dissociative hydrogen chemisorption is the most selective to GBL, so the existence of a correlation between both factors, which may be in line with the differences in exposed Ni^0 surface structure, can be hypothesized. In other words, the exposed Ni^0 phase on Ni/SiAl–PD has a much lower capacity for the dissociative H$_2$ chemisorption (per Ni^0 atom) than the one formed on Ni/Si–PD, which would be related with a different kind of metal surface structure on both catalysts. This could have some impact on the selective SA hydrogenolysis to GBL. However, the influence of the acid sites present on the support surface on hydrogenolysis reactions cannot be ruled out. It has been previously proposed that glycerol dehydration occurs through a C—OH bond hydrogenolysis mechanism that starts with the on-top glycol chemisorption on Lewis acid sites [44,45]. In a previous work, we determined that SiO$_2$–Al$_2$O$_3$ (Si/Al = 6.6) has mainly Lewis acid sites of varying strength on its surface [34]. Therefore, it is possible that the on-top chemisorption of SA occurs over the strongest Lewis acid sites at the metal-support interface through one of its C=O groups. This group could be then activated for the subsequent hydrogenation–hydrogenolysis by spillover of the H chemisorbed on the metal phase.

In summary, a metal Ni phase highly dispersed with a particle size between 3 and 6 nm, obtained by the precipitation–deposition method, is very active for the selective hydrogenolysis of SA into GBL. Instead, larger metal Ni particles having low interaction with the support were obtained using incipient wetness impregnation, which resulted less active and selective for conversion of SA into GBL. The support has also an important influence on the activity and the selectivity to the desired reaction. Yields and selectivities to GBL higher than 90% at almost 100% SA conversion were obtained with a Ni/SiO$_2$–Al$_2$O$_3$ catalyst prepared by precipitation–deposition. These values are higher than those obtained in a previous work with a Ni/SiO$_2$–Al$_2$O$_3$ catalyst prepared by incipient wetness impregnation: the maximum selectivity to GBL reached at 220 °C was 87%, approximately, but the SA conversion was less than 64% [34].

3.3. Temperature-programmed oxidation

In order to obtain more information about the catalysts deactivation observed during the catalytic tests, temperature-programmed oxidation (TPO) experiments were carried out with the used catalysts. In all of the cases, samples for TPO analyses were taken after a 185 min catalytic test.

The TPO profiles for Ni/Si–PD and Ni/SiAl–PD are shown in Fig. 8A and B, respectively. For both catalysts, TPO profiles display mainly a single peak of similar shape. The TPO profile corresponding to Ni/Si–PD used in reaction at 220 °C also shows a very small
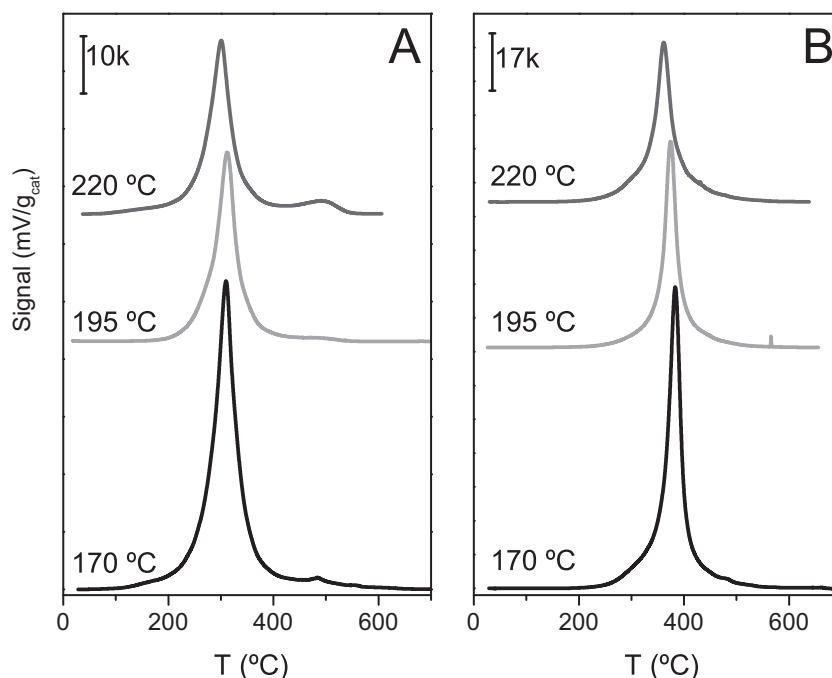
Fig. 8. Temperature-programmed oxidation profiles of the used catalysts after 185 min reaction at different temperatures. (A) Ni/Si–PD and (B) Ni/SiAl–PD. (P = 1 bar, W/F^0_{MA} = 12 g h mol^{-1}).

Table 4
Coke content (wt.%) determined from temperature-programmed oxidation after gas-phase maleic anhydride hydrogenation at different temperatures (P = 1bar, W/F^0_{MA} = 12ghmol^{-1}, reaction time: 185 min).

Catalyst	Reaction temperature (°C)		
	170	195	220
Ni/Si-I	1.6	n.d.	1.6
Ni/Si-PD	3.96	2.31	2.51
Ni/SiAl-PD	4.69	3.24	3.28

peak around 500 °C, that may be attributed to a more stable coke phase deposited on the support. However, its intensity is very low and almost negligible respect to the main signal at 300 °C. On the other hand, it is worth noting that the temperature of the maximum O_2 consumption shifts up to 20 °C to lower temperatures when the reaction temperature rises from 170 °C to 220 °C. Besides, TPO peak position is shifted from ca. 300 °C for Ni/Si–PD to almost 400 °C for Ni/SiAl–PD. This means that carbonaceous species deposited on Ni/SiAl–PD are more stable than the ones deposited on Ni/Si–PD, likely due to a stronger interaction with Ni/SiAl–PD surface than with the Ni/Si–PD one. This stronger interaction is in agreement with the assumption of the mechanism for SA hydrogenolysis to GBL involving its adsorption on Lewis acid sites surrounding the metallic Ni particles on Ni/SiAl–PD. As it was stated before, the SA → GBL sites are the ones suffering deactivation in both PD samples. So, in the case of Ni/SiAl–PD, the deactivating carbonaceous species would be deposited on the aforementioned acid sites, therefore being more stable than when they are deposited on the metal surface of Ni/Si–PD. It is worth mentioning that TPO profiles obtained for Ni/Si–I (not shown) are very similar in shape and position to those observed for Ni/Si–PD.

The total carbon deposited on the catalyst surface was quantified by numerical integration of the TPO profiles, and the results are shown in Table 4. It was found that total carbon amount is higher on catalysts prepared by PD (2.5–4%) than on Ni/Si–I (1.6%). This is consistent with the fact that PD catalysts show some deactivation while Ni/Si–I does not. In the case of Ni/Si–I, the total carbon deposited

was similar at 170 and 220 °C. Instead, for catalysts prepared by PD the amount of coke diminished when the reaction temperature was raised from 170 °C to 195 °C, and practically does not change between 195 and 220 °C. This is in agreement with the explanation proposed in Section 3.2 for the decay observed in SA conversion and GBL yield with time on stream (Figs. 5 and 6). It is more likely that the diminution in total carbon with temperature is due to the increase in the rate of hydrogenation and hydrogenolysis reactions of adsorbed coke precursors, which clean the catalyst surface. The rate increase of these surface-cleaning reactions with temperature would be higher than that of coke precursors deposition, resulting in a lower amount of deposited carbon as the reaction temperature is raised from 170 °C to 195 °C. In addition, the relative decrease in total carbon for Ni/SiAl–PD was lower than that for Ni/Si–PD indicating that the rate increase of cleaning reactions relative to coke deposition was also lower. This is in agreement with the residual activity observed for the PD catalysts and also with the evolutions with time on stream shown in Figs. 5 and 6. Similar behavior was previously observed with Cu/SiO$_2$ and Co/SiO$_2$ catalysts [32,33].

In summary, two effects were observed on the carbonaceous species deposition when reaction temperature was increased: a shift of the main TPO signal to lower temperatures, and a decrease in its intensity. Then, in agreement with the former discussion, it can be stated that carbonaceous species are located on the active sites of each catalyst, i.e., metal Ni particles on Ni/Si–PD and Lewis acid sites in contact with metal Ni on Ni/SiAl–PD, and migration to the support surface can be considered negligible.

3.4. Correlation of the characterization and catalytic activity results

All the Ni-based catalysts used in this work are very active in MA hydrogenation into SA. When the catalyst is prepared on SiO$_2$ by incipient wetness impregnation method (Ni/Si–I), a NiO phase with low or no interaction with the support is obtained after calcination. After complete reduction, the metallic Ni phase is comprised of large particles, in a wide range of sizes, formed by agglomeration of crystallites. This metal phase is active in the hydrogenolysis of SA

but gives low selectivity to GBL: similar amounts of GBL and PA are obtained with this catalyst. Besides, the maximum SA conversion reached with Ni/Si–I at 220 °C was about 65%.

When Ni/SiO$_2$ catalyst is prepared by precipitation–deposition (Ni/Si–PD), the Ni^{2+}-support interaction is much stronger than in the case of Ni/Si–I and a nickel hydrosilicate-like compound is formed on the support surface. This phase is more difficult to reduce than NiO, but the metallic Ni nanoparticles formed after reduction at 550 °C are homogeneously distributed in size and much smaller than on Ni/Si–I. The intrinsic activity of Ni/Si–PD is lower than that of Ni/Si–I but the exposed Ni^0 surface area of the former is much larger. As a consequence, the overall hydrogenolytic activity of Ni/Si–PD is higher than that of Ni/Si–I. In addition, these small metal Ni nanoparticles on Ni/Si–PD, strongly interacting with the SiO$_2$ surface, are more selective to GBL than the larger metal Ni particles formed on Ni/Si–I.

When the catalyst is prepared by precipitation–deposition of Ni over SiO$_2$–Al$_2$O$_3$ (Ni/SiAl–PD), the Ni^{2+}-support interaction is some weaker than that in Ni/Si–PD but stronger than that in Ni/Si–I. A nickel hydrosylicate-like compound is also formed, and the metallic Ni particles obtained after reduction at 500 °C are similar in size and shape than in the case of Ni/Si–PD. The specific hydrogenolytic activity of both samples prepared by PD is similar, but Ni/SiAl–PD shows a larger Ni^0 surface area resulting in a higher overall hydrogenolytic activity. In addition, a remarkably superior selectivity to GBL was also achieved, which can be explained considering: (1) structural differences in the exposed Ni^0 surface between both PD samples, since no electronic effect of SiO$_2$–Al$_2$O$_3$ on surface Ni^0 was evidenced from the XPS spectra but the amount of chemisorbed hydrogen per atom of metal Ni is much higher on Ni/Si–PD than on Ni/SiAl–PD; (2) intimate metal-Lewis acid sites interaction. On one hand, it may be possible that the medium Ni^{2+}-support interaction degree obtained when Ni is dispersed on the surface of SiO$_2$–Al$_2$O$_3$ is an optimum to reach such a high selectivity to GBL, even at the highest temperature used in this work. On the other hand, the presence of Lewis acid sites on the SiO$_2$–Al$_2$O$_3$ surface leads to consider an additional hydrogenolysis mechanism. Then, not only the preparation method but also the support nature would play a very important role on the type of active site exposed at the catalyst surface. On-top adsorption of SA throughout one C=O group on these surface Lewis acid sites, in intimate contact with the metal Ni nanoparticles, can yield GBL as a product through consecutive hydrogenation–hydrogenolysis by spillover of H$_2$ dissociatively chemisorbed on the metal phase. Then, the coexistence of metal Ni nanoparticles and Lewis acid sites in intimate contact would explain the higher selectivity to GBL of Ni/SiAl–PD respect to Ni/Si–PD. In addition, disparities in H$_2$ chemisorption capabilities support the existence of structural differences on the metal nanoparticles surface of both activated samples prepared by PD method. It is likely that SA hydrogenolysis into PA is less important over metal Ni nanoparticles on Ni/SiAl–PD than on Ni/Si–PD, what will contribute to increase selectivity to GBL. As a consequence, the highest yield and selectivity to GBL was obtained with Ni/SiAl–PD catalyst: more than 90% even at 100% of SA conversion, which are greater than those obtained in a previous work with a Ni/SiO$_2$–Al$_2$O$_3$ prepared by incipient wetness impregnation [34].

The amount and stability of carbonaceous compounds deposited on the catalyst surfaces are also different for each used sample and follow the pattern: Ni/SiAl–PD > Ni/Si–PD > Ni/Si–I. This trend could be also related with both the differences on surface structure of metal particles and the acidity of support surfaces. On the other hand, a deactivation with residual activity was observed for both catalysts prepared by the precipitation–deposition method, attributable to competitive carbonaceous species deposition and regeneration by hydrogenation–hydrogenolysis of these compounds. Ni/Si–PD reached this steady state faster than Ni/SiAl–PD,

what may be explained by considering that the relative rates of these competitive reactions are different on each surface. This deactivation with residual activity was not observed with Ni/Si–I. These differences in deactivation–regeneration behavior are also evidence that interaction of reactant molecules and active surface is rather different on each of the catalysts used in this work due to important differences on the surface structures.

4. Conclusions

The preparation method and support nature have a strong influence on physicochemical properties and catalytic performance of Ni-based catalysts used in the gas-phase hydrogenation of maleic anhydride at atmospheric pressure. The highest selectivity to GBL in this work, between 90% and 95% at total reactant conversion, was obtained with a Ni-based catalyst supported on SiO$_2$–Al$_2$O$_3$ prepared by the precipitation–deposition method at constant pH. This catalytic performance was significantly superior to that obtained in a previous work with a Ni/SiO$_2$–Al$_2$O$_3$ catalyst prepared by incipient wetness impregnation.

A Ni/SiO$_2$ catalyst prepared by incipient wetness impregnation has a metal Ni phase constituted by large particles, with a non-uniform size distribution, and low interaction with the support. On the other hand, constant-pH precipitation-deposition method leads to Ni-based catalysts with highly dispersed metal nanoparticles and strong interaction with the support. These catalysts are more active for the selective gas-phase hydrogenation of maleic anhydride to γ-butyrolactone than that prepared by the incipient wetness impregnation method.

The outstanding performance of the Ni/SiO$_2$–Al$_2$O$_3$ catalyst prepared by precipitation–deposition at constant pH is attributed to the nature of its active phase, consisting of metal nickel nanoparticles, 3–6 nm in size, uniformly dispersed and interacting with Lewis acid sites of varying strength present on the support surface. The adsorption of succinic anhydride over this type of catalytic surface favors its selective hydrogenolysis to γ-butyrolactone. The assumption of different surfaces on both catalysts prepared by the precipitation–deposition method is also supported by: (1) the amounts of irreversibly chemisorbed hydrogen relative to the exposed metal Ni surface; (2) the presence of Lewis sites on the SiO$_2$–Al$_2$O$_3$ surface but not on the SiO$_2$ surface; (3) the differences on the deactivation–regeneration behavior during the catalytic runs; (4) the differences of the stability of the carbonaceous compounds formed over each metal surface.

Acknowledgements

References

[1] W. Schwarz, J. Schossig, R. Rossbacher, H. Höke, Butyrolactone, in: Ullmann's Encyclopedia of Industrial Chemistry, Weinheim, 2005.
[2] B. Zhang, Y. Zhu, G. Ding, H. Zheng, Y. Li, Appl. Catal. A: Gen. 443 (2012) 191–201.
[3] G. Budroni, A. Corma, J. Catal. 257 (2008) 403–408.
[4] Y. Yu, Y. Guo, W. Zhan, Y. Guo, Y. Wang, G. Lu, J. Mol. Catal. A: Chem. 392 (2014) 1–7.
[5] J.-Y. Huang, X.-J. Liu, X.-L. Kang, Z.-X. Yu, T.-T. Xu, W.-H. Qiu, J. Power Sour. 189 (2009) 458–461.
[6] N. Wongittharom, C.-H. Wang, Y.-C. Wang, G.T.-K. Fey, H.-Y. Li, T.-Y. Wu, T.-C. Lee, J.-K. Chang, J. Power Sour. 260 (2014) 268–275.

[7] M.V. Reppe, R. Keissner, US Patent, 2232867 (1941).
[8] C. Miyazawa, K. Takahashi, H. Kameo, S. Isogai, M. Otake, US Patent, 5047561 (1991).
[9] A.G. Hiles, M.W.M. Tuck, US Patent, 5254758 (1993).
[10] T. Asano, J. Kanetaka, K. Miyake, H. Sugiura, US Patent, 3492314 (1970).
[11] G.L. Castiglioni, C. Fumagalli, A.S. Alessandro, US Patent, 6492535 (2002).
[12] H. Jeong, T.H. Kim, K.I. Kim, S.H. Cho, Fuel Process. Technol. 87 (2006) 497–503.
[13] U. Herrmann, G. Emig, Ind. Eng. Chem. Res. 36 (1997) 2885–2896.
[14] Y. Hara, H. Kusaka, H. Inagaki, K. Takahashi, K. Wada, J. Catal. 194 (2000) 188–197.
[15] S.M. Jung, E. Godard, S.Y. Jung, K.-C. Park, J.U. Choi, Catal. Today 87 (2003) 171–177.
[16] S.M. Jung, E. Godard, S.Y. Jung, K.-C. Park, J.U. Choi, J. Mol. Catal. A: Chem. 198 (2003) 297–302.
[17] S.H. Vaidya, C.V. Rode, R.V. Chaudhari, Catal. Commun. 8 (2007) 340–344.
[18] M. Aghaziarati, M. Soltanieh, M. Kazemeini, N. Khandan, Catal. Commun. 9 (2008) 2195–2200.
[19] J. Li, W.P. Tian, X. Wang, L. Shi, Chem. Eng. J. 175 (2011) 417–422.
[20] Y. Feng, H. Yin, A. Wang, T. Xie, T. Jiang, Appl. Catal. A: Gen. 425–426 (2012) 205–212.
[21] M. Messori, A. Vaccari, J. Catal. 150 (1994) 177–185.
[22] G.L. Castiglioni, A. Vaccari, G. Fierro, M. Inversi, M. Lo Jacono, G. Minelli, I. Pettiti, P. Porta, M. Gazzano, Appl. Catal. A: Gen. 123 (1995) 123–144.
[23] G. Castiglioni, M. Ferrari, A. Guercio, A. Vaccari, R. Lancia, C. Fumagalli, Catal. Today 27 (1996) 181–186.
[24] C. Ohlinger, B. Kraushaar-Czarnetzki, Chem. Eng. Sci. 58 (2003) 1453–1461.
[25] Y. Zhu, G. Zhao, J. Chang, J. Yang, H. Zheng, H. Xiang, Y. Li, Catal. Lett. 96 (2004) 123–127.
[26] R. Zhang, H. Yin, D. Zhang, L. Qi, H. Lu, Y. Shen, T. Jiang, Chem. Eng. J. 140 (2008) 488–496.
[27] Y. Yu, Y. Guo, W. Zhan, Y. Guo, Y. Wang, Y. Wang, Z. Zhang, G. Lu, J. Mol. Catal. A: Chem. 337 (2011) 77–81.
[28] D. Gao, Y. Feng, H. Yin, A. Wang, T. Jiang, Chem. Eng. J. 233 (2013) 349–359.
[29] W. Huo, C. Xzhang, H. Yuan, M. Jia, C. Ning, Y. Tang, Y. Zhang, J. Luo, Z. Wang, W. Zhang, J. Ind. Eng. Chem. (2014), http://dx.doi.org/10.1016/j.jiec.2014.01.012
[30] U.R. Pillai, E. Sahle-Demessie, D. Young, Appl. Catal. B: Environ. 43 (2003) 131–138.
[31] Q. Wang, H. Cheng, R. Liu, J. Hao, Y. Yu, F. Zhao, Catal. Today 148 (2009) 368–372.
[32] C.I. Meyer, A.J. Marchi, A. Monzon, T.F. Garetto, Appl. Catal. A: Gen. 367 (2009) 122–129.
[33] C.I. Meyer, S.A. Regenhardt, A.J. Marchi, T.F. Garetto, Appl. Catal. A: Gen. 417–418 (2012) 59–65.
[34] S.A. Regenhardt, C.I. Meyer, T.F. Garetto, A.J. Marchi, Appl. Catal. A: Gen. 449 (2012) 81–87.
[35] C.I. Meyer, S.A. Regenhardt, M.E. Bertone, A.J. Marchi, T.F. Garetto, Catal. Lett. 143 (2013).
[36] J.A. van Dillen, J.W. Geus, L.A.M. Hermans, J. van der Meijden, Proceedings of the 7th International Congress on Catalysis, in: P.B. Bond (Ed.), The Chemical Society, London, 1976, pp. 677–685.
[37] M. Montes, C.H. Penneman de Bosscheyde, B.K. Hodnett, F. Delannay, P. Grange, B. Delmon, Appl. Catal. 12 (1984) 309–330.
[38] A. Gil, A. Díaz, L.M. Gandía, M. Montes, Appl. Catal. A: Gen. 109 (1994) 167–179.
[39] A.J. Majewski, J. Wood, W. Bujalski, Int. J. Hydrog. Energy 38 (2013) 14531–14541.
[40] S.C. Fung, C.A. Querini, J. Catal. 138 (1992) 240–248.
[41] R. Frety, L. Tournayan, M. Primet, G. Bergeret, M. Guenin, J. Baumgartner, A. Borgna, J. Chem. Soc. Faraday Trans. 89 (1993) 3313–3318.
[42] C. Plana, S. Amenise, A. Monzón, E. García-Bordejé, J. Catal. 275 (2010) 228–235.
[43] M.V. Bykova, D. Yu. Ermakov, V.V. Kaichev, O.A. Bulavchenko, A.A. Saraev, M. Yu Lebedev, V.A. Yakovlev, Appl. Catal. B: Environ. 113–114 (2012) 296–307.
[44] S. Xia, Z. Yuan, L. Wang, P. Chen, Z. Hou, Appl. Catal. A: Gen. 403 (2011) 173–182.
[45] T. Miyazawa, S. Koso, K. Kunimori, K. Tomishige, Appl. Catal. A: Gen. 318 (2007) 244–251.